COUPLED MECHANICAL AND ELECTROMAGNETIC MODELING OF EDDY CURRENT SENSORS

NIDHAL JAMIA[1*], MICHAEL I. FRISWELL[1], SAMI EL-BORGI[2] AND PRAKASH RAJENDRAN[2]

[1] College of Engineering, Swansea University
Bay Campus, Swansea SA1 8EN, United Kingdom
e-mail: 842543@swansea.ac.uk, web page: http://www.swansea.ac.uk/

[2] Texas A&M University at Qatar, Mechanical Engineering Program,
Engineering Building, P.O. Box 23874, Education City, Doha, Qatar
e-mail: sami.el_borgi@qatar.tamu.edu, web page: http://www.qatar.tamu.edu/

Key words: Rotating bladed disk, blade tip-timing, eddy current sensors, blade tip clearance, coupled mechanical and electromagnetic problem.

Abstract. To effectively monitor the vibration of blades in a rotating machine, a non-contacting method called blade tip-timing (BTT) has been used. The method is based on the analysis of the differential arrival times of the blades at sensors mounted on the stator to characterize the vibration amplitude and frequency of the blades. These sensors can also provide blade tip clearance measurement. A combination of these data can provide a robust condition monitoring approach for the early detection of blade cracks.
Eddy current sensors (ECS) have shown great potential to assess the health of an engine without any need for direct access to the blade and therefore they are insensitive to the presence of any type of contaminant. Also, both tip timing and tip clearance of each blade could be measured by these sensors in real time and at high resolution.
ECSs measure the magnetic field caused by eddy currents during the blade motion, and hence are a coupled mechanical and electromagnetic problem. An ECS on the casing of a machine has been modeled to fully understand how the dynamic response of the blade is measured by the sensors. Detailed 2-D and 3-D modeling and simulation of a rotating simplified bladed disk passing an ECS is presented.
The effect of the variation of the rotation speed and the gap between the sensor and the blade tip on the accuracy of the measurement is investigated. Such an analysis will enable the reliable monitoring of blade damage during engine operation.

1 INTRODUCTION

In turbomachinery, severe vibratory loads may lead to blade failures and therefore the total failure of the engine. Maintenance of the rotating machine is very important and has a tremendous impact on the life cycle cost of the engine. To obtain the best efficiency, an intelligent assessment is necessary for early damage diagnosis and condition based maintenance activities. Different monitoring techniques have been developed using sensors in the casing

around the rotating part to measure and estimate the time of the arrival (ToA) of the blade tips passing by the sensors. In the 1960s, Fragman et al. [1] developed a contact method where the measurement of rotating blade responses was performed by means of blade mounted strain gauges. This method has several shortcomings such as time and cost, and the low resistance to the harsh environment found inside the machine. As an alternative to this method, many investigators have considered contactless methods to monitor blade vibrations in the rotating machinery due to the non-intrusive and easy installation of sensors which allows prompt detection of potential cracks. One of the well-known contactless method is the Blade Tip Timing (BTT) approach, which estimates the blade vibration that is crucial in the assessment of machine operation and the prediction of blade failure due to fatigue [2]. The concept of this method relies on using a number of probes fixed to a casing of the machine to detect the blade tip as it passes by the probes. Then, the difference between the time of arrival (ToA) of non-vibrating and vibrating blades leads to the estimation of the vibration displacement utilized to identify vibration parameters [3].

During the early 1970s, Zablotsky and Korostelev ([4] and [5]) introduced the first non-contact measurement based on their own device to measure vibration called ELURA. This technique was extended by Heath and Imregun [6] based on an improved formulation to extract the blade arrival times using optical laser probes. Dimitriadis et al. [2] simulated data from traditional BTT tests of rotating blades. They performed a qualitative analysis of different phenomena that can affect the identification of blade vibration parameters such as mistuning or coupling. A modal parameter identification of rotating machine blades was presented by Salhi et al. [7] using a BTT data. Liu and Jiang [8] monitored the blade vibration of a rotating machinery test rig using the BTT method. They proposed a method to improve the accuracy of the measurements in the presence of torsional vibration. Similarly, Madhavan et al. [9] conducted an experiment to monitor the vibration measurement using the BTT technique. Therefore, the focus in the previous researches has been mainly on the experiment work to describe the BTT method.

Several sensing technologies have been proposed to monitor blade positions in turbomachinery relying on capacitance, inductance, optics, microwaves and eddy-currents. The focus in this paper will be mainly on the ECS due to its potential to assess the health of a machine without any need for direct access to the blade (e.g. the possibility to monitor through the casing) and therefore they are insensitive to the presence of any type of contaminant. Also, both tip timing and tip clearance of each blade could be measured by these sensors in real time and at high resolution. Dowell and Sylvester [10] described the physical principles of ECSs and the approach used to develop a health management program for turbomachinery. In addition, Lackner [11] assembled a test rig of three spinning test blades to test the ability of ECSs in a simulated gas turbine environment, he showed that ECSs could mitigate the drawbacks of other types of sensors, such as capacitive sensors. The arrival times of a rotor blade based on ECSs have been measured by Chana and Cardwell [12] in various machine trials to evaluate the ability of these sensors to detect pre-existing damage and to capture dynamic foreign object damage events. More recently, Mandache et al. [13] developed a pulsed eddy current technology to detect the blade and disk damage through the machine casing based on monitoring the blade tip displacement.

The emphasis in the existing literature was on the experimental side more than the modeling side. Therefore, a detailed model of the use of ECS in blade tip timing is required for further development of BTT systems and in order to increase the accuracy of the timing measurement. In this paper, 2-D and 3-D models of a simple rotating bladed disk passing active and passive ECSs are implemented using the COMSOL Multiphysics software to investigate the accuracy of the timing measurement when the blades pass by the sensor. The effect of the rotation speed and the tip clearance between the blade tip and the sensor on the sensor output is investigated.

2 BASIC THEORY OF AN ECS TO ASSESS A MOVING TARGET

2.1 Principe of eddy current sensor

In this section the concept of eddy current monitoring is described. If a conductive target moves through a permanent magnet field or an alternating magnetic field is acting on a moving target, induced eddy currents are generated and detected by the coil system of an ECS. These two cases correspond to a passive eddy current sensor (P-ECS) and active eddy current sensor (A-ECS) that have both been used for BTT measurements. Starting with the case of A-ECS, the operating principles are understood as follows [13]. An alternating current running through a coil of ECS generates a primary time-varying magnetic field formed around the coil. If an electrically conducting target is moving past it, eddy currents are generated and induced in the target due to Faraday's law of induction. A secondary magnetic field is generated by these induced currents and acts against the primary magnetic field as shown in Figure 1. This results in a variation of the coil's impedance which is captured by the sensor. Measuring this discrepancy of coil impedance will reveal particular information, such as the gap between the sensor and the target, or the vibration of the target tip.
A P-ECS follows similar approach to an A-ECS, except that the primary magnetic field is permanent and the induced eddy currents are generated by the motion of the target. Therefore, the sensor picks up the secondary magnetic field generated by these eddy currents. This type of sensor is not considered as a displacement sensor since it measures velocity and hence it does work well for BTT where the blade is always moving past the sensor.

2.2 Modeling the eddy current's effect in a moving target

In this section, the effect of the eddy current in a moving target is modeled using the vector and scalar potential terms. To describe the electro-magnetic field in terms of sources, Maxwell's equations (Eqs. (1)-(4)) along with constitutive equations (Eqs. (5) and (6)) and the magnetic and electric material properties of the moving target are used as [14-15]:

$$\nabla \times H = J + \frac{\partial D}{\partial t} \tag{1}$$

$$\nabla \times E = -\frac{\partial B}{\partial t} \tag{2}$$

$$\nabla \cdot D = \rho \tag{3}$$

$$\nabla \cdot B = 0 \tag{4}$$

$$D = \varepsilon E \tag{5}$$

$$B = \mu H \tag{6}$$

where H is the magnetic field strength, B is the magnetic flux density, E is the electric field, D is the displacement flux density, J is the current density, ρ is the charge density, μ is the magnetic permeability and ε is the electric permittivity of the medium.
In the case of an eddy current sensor monitoring a conductive target, the total electric current generated is given by

$$J = J_t + J_s, \tag{7}$$

where J_t is the electric current density in the conductive target and J_s is the external electric current density induced in the sensor. Following Ohm's law for a moving conductor, along with the presence of the magnetic field, the eddy current generated in the target is defined as

$$J_t = \sigma(E + v \times B) \tag{8}$$

where v is the velocity of the target and σ is the conductivity of the target's medium.
Satisfying two of Maxwell's equations, Eqs. (2) and (4), the magnetic vector potential A and the scalar potential φ are defined as

$$E = -\nabla\varphi - \frac{\partial A}{\partial t} \tag{9}$$

$$B = \nabla \times \mathrm{A} \tag{10}$$

Since the eddy current problem is a magneto-quasi-static problem [16], the displacement current can be ignored, i.e. $\frac{\partial D}{\partial t} \approx 0$. Therefore, substituting Eqs. (6-10) into Eq. (1) yields

$$\nabla \times B = \mu J + \sigma\mu(E + v \times B) \tag{11}$$

By rearranging the terms in Eq. (11) and replacing the electric field and magnetic flux density by their expressions in Eqs. (9) and (10), we obtain, in terms of A and φ, the following magnetic governing equation

$$\nabla \times (\nabla \times \mathrm{A}) - \mu\sigma\left(-\nabla\varphi - \frac{\partial A}{\partial t} + v \times (\nabla \times \mathrm{A})\right) = \mu J_s \tag{12}$$

3 NUMERICAL METHOD FOR TESTING THE BTT USING AN ECS

In this section, a simulation of the distribution of an eddy current by a passive and active ECS in a simple rotating bladed disk is described. This presents a first step towards realistic geometries where it is complicated to change parameters easily. To achieve this task, a commercial FEA software package, COMSOL Multiphysics® [17], was used.

3.1 Geometry of 2-D and 3-D model of a simple bladed disk

A 2-D and 3-D geometry of the model were created using the COMSOL Multiphysics® software. The geometry of the two models is shown in Figure 2 and was generated based on the design parameters given in Table 1. The bladed disk is composed of a disk and 4 simple rectangular blades. A rectangular ECS is fixed at a distance $\boldsymbol{\delta}$ which equals the gap between the blade tip and the sensor. The blades, disk and sensor are assumed to be solid aluminium.

Table 1: Specifications of the bladed disk configuration

Name	Expression	Value	Description
Ω	*2000[1/min]*	*33.333 1/s*	Rotational speed of the rotor
R	*0.1[m]*	*0.1 m*	Radius of the rotor hub
l	*0.1[m]*	*0.1 m*	Blade length
b	*0.005[m]*	*0.005 m*	Blade width
a	*0.003[m]*	*0.003 m*	Overlap of blade into the disk
w_s	*1 [cm]*	*0.002 m*	Sensor width
l_s	*4 [cm]*	*0.005 m*	Sensor Length
δ	*10 [mm]*	*0.005 m*	Gap between Sensor and Blade tip
R_a	$R + l - a + \delta/2$	*0.1995 m*	Radius of Moving surrounding air circle
R_s	$1.25 * R_a$	*0.2495 m*	Radius of Static surrounding air circle
Vcoil	*1e-5[V]*	*1e-5 V*	Coil excitation for P-ECS
f_0	$1000 * \Omega$	*16667 Hz*	Coil excitation frequency for A-ECS

3.2 Modeling the coupled mechanical and electro-magnetic problem using 2-D and 3-D models

3.2.1 Passive ECS model

The 2-D and 3-D domains are discretized by cutting the geometry along the air gap into two parts: one containing the static part of the model (the sensor and surrounding air), and the other containing the moving part (i.e. the disk, the blades and the surrounding air) as shown in Figure 3. The two parts are then meshed separately. Triangular elements were used in the discretization of the 2-D model while in the 3-D model, tetrahedral elements were used. The total number of elements used was 20620 elements in the 2-D model and 48669 elements for the 3-D model as shown in Figure 4. The static part remains stationary while the moving part rotates. These two parts with the corresponding meshes always stay in contact at the cut boundary. The COMSOL software enables the moving mesh for the rotating part and guarantees suitable transformations of the electromagnetic field. In the 2-D model, the COMSOL interface applies Ampere's law to all domains, while in the 3-D model, Ampere's law is applied only for the conductive domains (e.g. bladed disk and sensor). For the free-current domain, such as the surrounding air in the 3-D model, a magnetic flux conservation feature is applied based on the assumption that the magnetic field is curl free in the no-current region and therefore there is an important decrease of computational time.

3.2.2 Active ECS model

This model is based on measuring the change in the coil impedance which is related to the gap between the sensor and the target, and hence the sensor output gives the relative displacement. Therefore, compared to the P-ECS model, the continuous rotation approach is ignored and replaced with a series of blade positions using a sweep of geometry parameter defined as

$$rot_{angle} = t_{para} * \Omega * 2\pi \ \ (rad) \tag{13}$$

where t_{para} is a parametric time and the blade will rotate with respect to this time. Then, the model is solved as a series of frequency domain studies whilst rotating the blades in the geometry via a Parametric Sweep. A frequency domain study defines that an alternative current is used for the coil excitation oscillating at a parameter f_0. This excitation has been set to be 1000 times the spinning blade, to ensure that the quasi-static approximation is valid. A very fine mesh is used for the fan and the coil. The mesh in the blades has been heavily refined to resolve the currents well. Finally, 16235 triangular elements have been used in the 2-D model and 54412 tetrahedral elements for the 3-D model, as shown in Figure 5.

For both models described, a coil feature from the Magnetic Fields interface in COMSOL software was assigned to rectangle 2, as shown in Figure 2, to model the sensor as a conductor subject to an externally applied current or voltage. This feature transforms the applied excitation into local quantities (e.g. electric field and electric current density), and calculates the lumped parameter of interest such as impedance in this case. In addition, due to convergence issues in the 3-D model, the current value in the coil was ramped from a low value using a smoothed step function. Finally, the boundary conditions were fixed by the COMSOL interface, considering continuity of the magnetic potential along the blades and applying the quasi-static approximation where the displacement current density is ignored.

4 SIMULATION RESULTS OF THE ROTATING BLADED DISK USING P-ECS AND A-ECS

All results shown in this section were generated by the COMSOL software for the fixed geometric parameters in Table 1, apart from the parameter that is explicitly varied.

4.1 Validation of results between 2-D and 3-D model

A comparison of the coil output currents corresponding to the 2-D and 3-D models for the P-ECS model, is generated for the same geometric parameters and shown in Figure 6. The same comparison was performed for the A-ECS and is shown in Figure 7. The small difference between the two models is probably due to the effect of the thickness of the disk in the 3-D model. Overall, there is excellent agreement between the two models for P-ECS and A-ECS, giving confidence in the equivalence of the 2-D and 3-D models in this configuration. The 3-D models requires significant computational resources (around 12-16 hours per simulation), and hence the following results are obtained from the 2-D model.

4.2 Simulations for the rotating bladed disk and ECS

In this section, a stationary and time-dependent analyses for an interval of time of 0.36 seconds and at a rotational speed of the rotor equal to 2000 rev/min were performed for the P-ECS model. Regarding the A-ECS model, it is solved for a full period of rotation of the bladed disk $T_0 = 1/\Omega$, for 600 time steps within that time interval.

Figure 8 shows the surface plot of the magnetic flux density's norm for the 2-D model corresponding to the P-ECS and A-ECS cases at the instant when one of the blades passes by the sensor. The magnetic vector potential is also shown by magnetic flux lines induced thorough the plane of the bladed disk. We can notice a variation in the induced magnetic flux lines. This variation is due to the interference between the primary magnetic field generated by the ECS and the secondary magnetic field generated by the moving blades past the sensor. This agrees

with the concept of ECSs described in Section 2.1. Figure 9a shows the corresponding coil voltage captured by the P-ECS when a blade passes by it in the 2-D model. Figure 9b shows the variation of the impedance in the coil due to passing of the blades. As observed for both models, a signal peak is obtained every time a conducting blade enters the field of the sensor which alters the magnetic field through the induced eddy currents in the blades. This describes clearly the behavior of an ECS; based on a reference voltage which will correspond to a known position on the blade, the time of blade passing can be determined. This gives information about the time of arrival of the blade at the sensor probe. In addition, the shape of a single peak corresponding to the P-ECS case, gives a reference to determine when the blade is positioned at the middle of the sensor which gives more detail about the blade positon compared to the shape of signal corresponding to the A-ECS. Figure 10 shows the effect of the variation of the gap (i.e. the distance separating the blade tip and the surface of the sensor during the rotation of the bladed disk) on the sensor output. There is a clear decrease in the signal amplitude with increasing gap between the sensor and blade tip. This shows the sensitivity of the ECS to small distance variations. Finally, Figure 11 shows the effect of the rotational velocity of the bladed disk on the sensor output. The output curves have been shifted so that the blade passes the sensor at the same time. The variation of signal amplitude is more important for the P-ECS than the A-ECS which agree with the fact that the P-ECS is not a displacement sensor and is affected by the target speed while the velocity doesn't affect the A-ECS output. This sensitivity shows that the P-ECS could be more efficient for the BTT measurement.

5 CONCLUSION

This paper has simulated a rotating bladed disk of simple geometry monitored by passive and active eddy current sensors. The aim was to simulate the measurement process used for blade tip timing using eddy current sensors. Eddy current sensors have been considered in this paper due to their robustness in harsh environments. The governing equations modeling the magneto electric field of a moving target have been described for a quasi-static problem. A detailed description of the geometry of the 2-D and 3-D models were described, together with the meshing difficulties encountered due to the rotation, and the physics of the coupled problem of mechanical and electro-magnetic fields. The simulations gave sensor outputs that correspond to those measured and reported in the literature for P-ECS and A-ECS. The parameter studies showed that the eddy current sensor output is sensitive to the air gap and the sensor location, as well as to the rotational speed of the system. This sensitivity can help to understand the errors that could be introduced and the time of blade passing can be estimated more accurately by taking in consideration these effects. Moreover, this modeling approach can be utilized to design and optimize blade tip timing systems with multiple sensors and complex geometries; such studies will be the subject of future research.

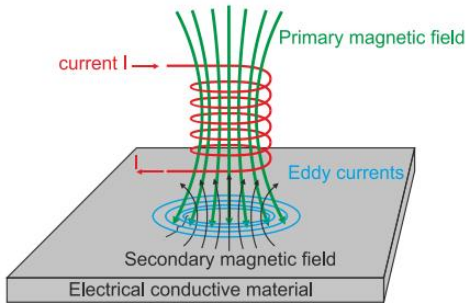

Figure 1: The eddy current sensor concept (adapted from [16]).

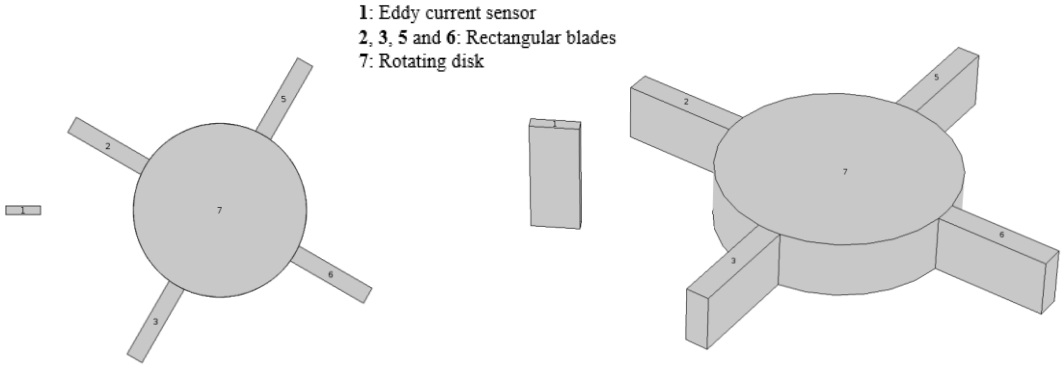

(a) (b)

Figure 2: The geometry of the (a) 2-D model (b) 3-D model

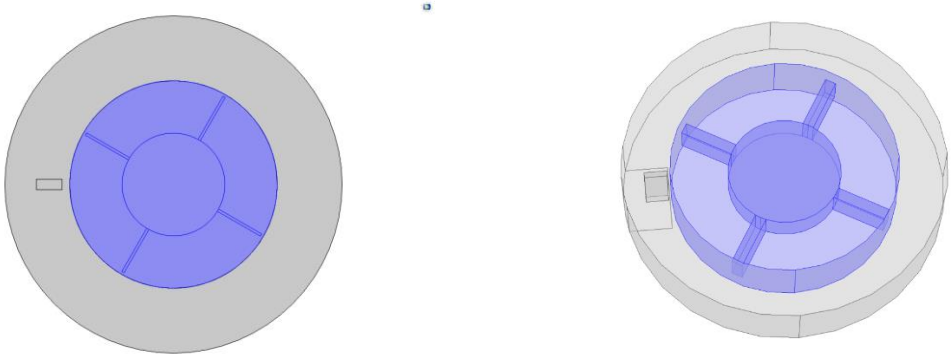

(a) (b)

Figure 3: The static and moving parts of the geometry for the (a) 2-D model (b) 3-D model for P-ECS case

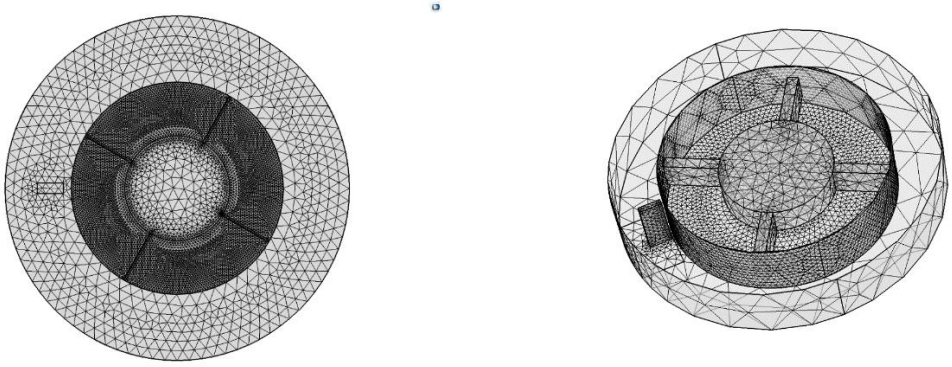

(a) (b)

Figure 4: Meshing details of the (a) 2-D models (b) 3-D model for P-ECS case

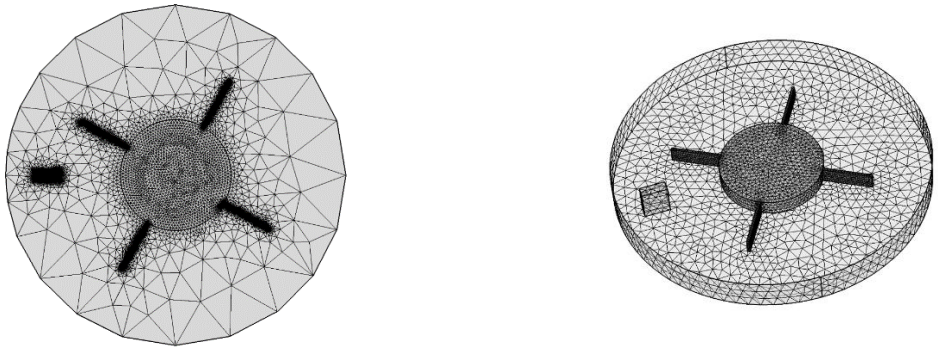

(a) (b)

Figure 5: Meshing details of the (a) 2-D models (b) 3-D model for A-ECS case

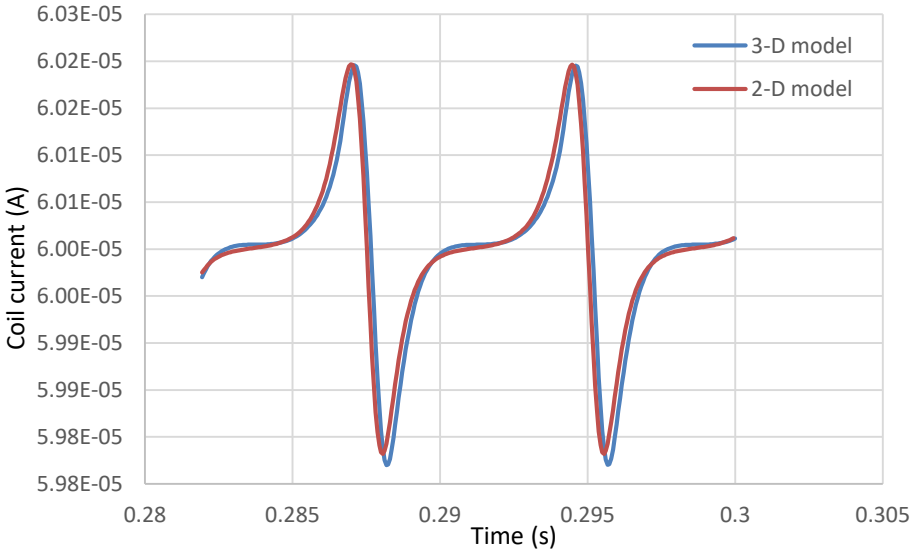

Figure 6: Comparison of the coil current signal of 2-D and 3-D models for the P-ECS case

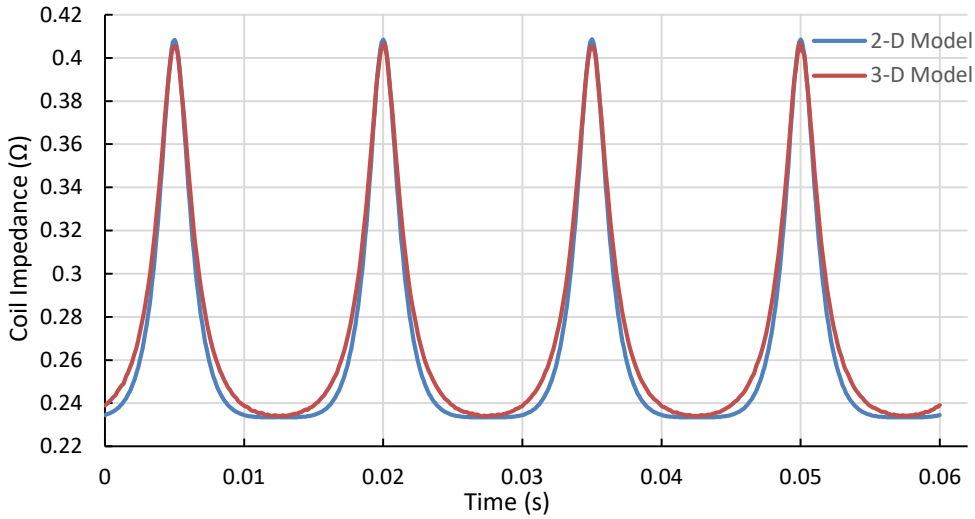

Figure 7: Comparison of the Impedance variation in the coil for the 2-D and 3-D models for the A-ECS case

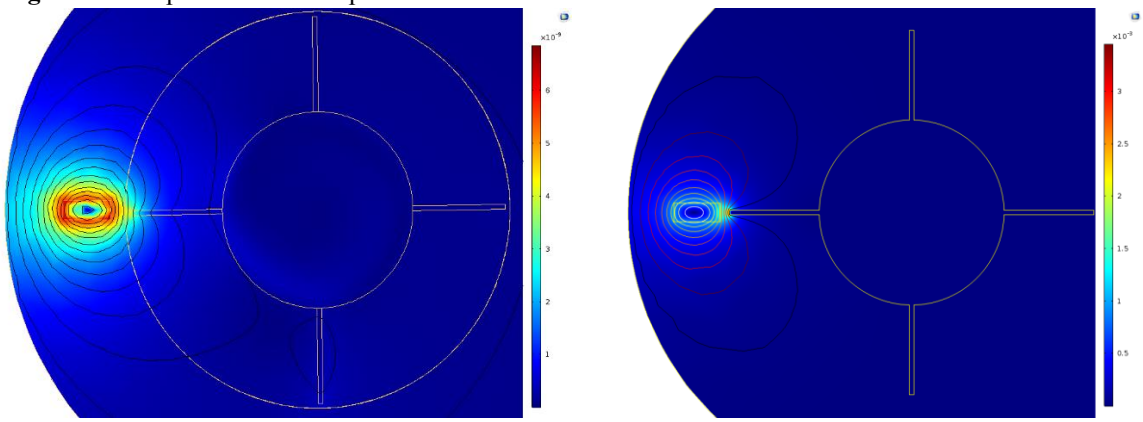

(a) (b)

Figure 8: Magnetic flux density norm (Surface) and Magnetic vector potential Z-component (Contour) for the 2-D model at (a) t = 0.35016s for P-ECS case (b) at t = 0.05s for A-ECS case

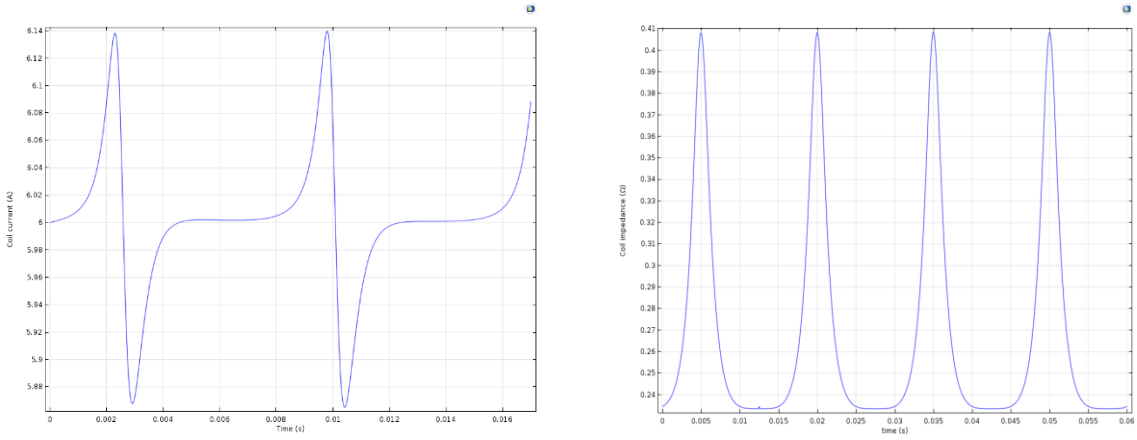

(a) (b)

Figure 9: Output of the ECS corresponding to the 2-D model for the case of (a) P-ECS (b) A-ECS

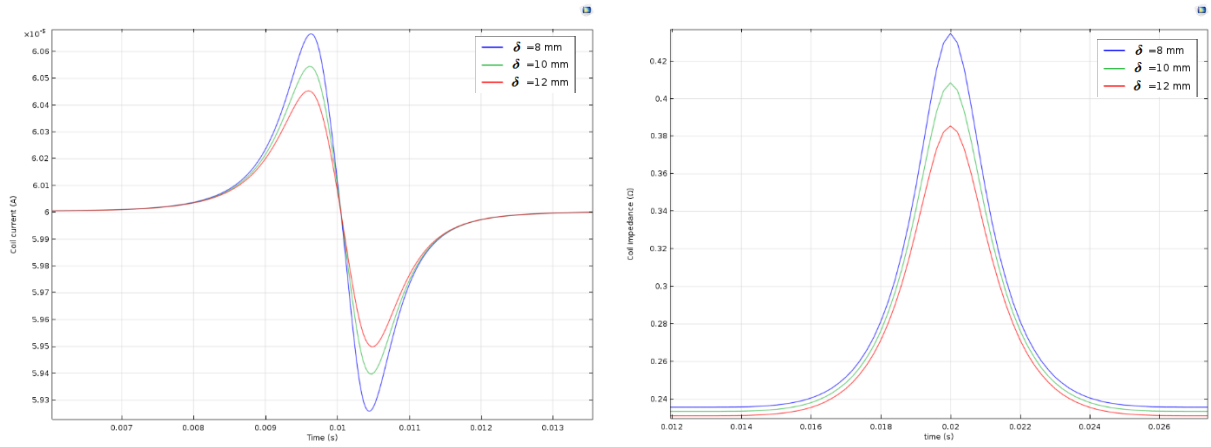

(a) (b)

Figure 10: The induced voltage in the sensor with time for different blade gaps for (a) A-ECS case (b) P-ECS case

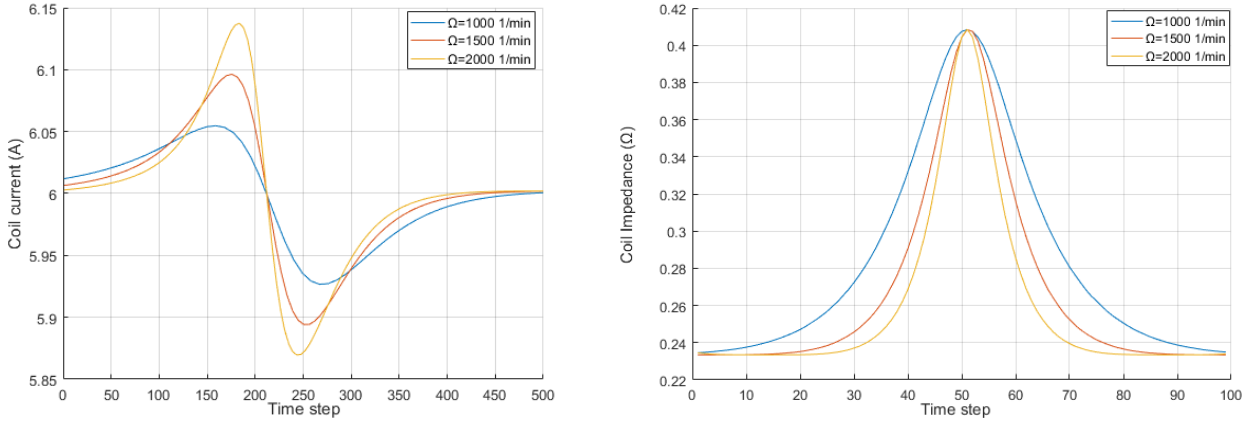

(a) (b)

Figure 11: The induced voltage in the sensor with time for different rotational speeds for (a) A-ECS case (b) P-ECS case (curves shifted to a common point)

ACKNOWLEDGEMENTS

The authors gratefully acknowledge the support of the Qatar National Research Fund through grant number NPRP 7-1153-2-432.

REFERENCES

[1] Fangman, C., Zastrow, V., Bobeck, J. High-speed-turbocharger blade-vibration measurement, Experimental Mechanics, Vol. 7, No. 1, (1967), pp. 19A-21A.

[2] Georgiev, V., Holík, M., Kraus, V., Krutina, A., Kubín, Z., Liška, J., Poupa, M. The Blade Flutter Measurement Based on the Blade Tip Timing Method, Proceedings of the 15th WSEAS International Conference on Systems, Corfu Island, Greece, 2011 July 14–16, pp. 270–275.

[3] Dimitriadis, G., Carrington, I.B., Wright, J.R., Cooper, J.E. Blade-tip timing measurement of synchronous vibrations of rotating bladed assemblies, Mechanical Systems and Signal Processing, Vol. 16, No. 4, (2002), pp. 599-622.

[4] Zablotskiy, I.Y. and Korostelev, Y.A. Measurement of Resonance Vibrations of Turbine Blades with the Elura Device, Energomashinostroneniye, No. 2, (1970), pp. 36-39.
[5] Zablotskiy, I.Y., Korostelev, Y.A, Sviblov, L.B. Contactless Measuring of Vibrations in the Rotor Blades of Turbines, Foreign Technology Division, WP-AFB, Ohio, (1974), 19 pages.
[6] Heath, S. and Imregun, M. An improved single-parameter tip-timing method for turbomachinery blade vibration measurements using optical laser probes, International Journal Mechanical Science, Vol. 38, No. 10, (1996), pp. 1047-1058.
[7] Salhi, B., Lardies, J., Berthillier, M., Voinis, P., Bodel, C. Modal parameter identification of mistuned bladed disks using tip timing data, Journal of Sound and Vibration, Vol. 314, No. (3-5), (2008), 885–906.
[8] Liu, C. and Jiang, D. Improved Blade Tip Timing in Blade Vibration Monitoring with Torsional Vibration of the Rotor, Journal of Physics: Conference Series, Vol. 364, (2012), Conf. (1).
[9] Madhavan, S., Jain, R., Sujatha, C., Sekhar A.S. Vibration based damage detection of rotor blades in a gas turbine engine, Engineering Failure Analysis Vol. 46, (2014), pp. 26–39.
[10] Dowell, M. and Sylvester, G. Turbomachinery Prognostics and Health Management via Eddy Current Sensing: Current Developments, Proceedings of the 1999 IEEE Aerospace Conference, Snowmass at Aspen, CO, 1999 March 6-13, Volume 3 (1999), pp. 1-9.
[11] Lackner, M. Vibration and Crack Detection in Gas Turbine Engine Compressor Blades using Eddy Current Sensors, Master of Science thesis, Massachusetts Institute of technology, Department of Aeronautics and Astronautics, Cambridge (2004).
[12] Chana, K.S. and Cardwell, D.N. The Use of Eddy Current Sensor Based Blade Tip Timing for FOD Detection, Proceedings of the ASME Turbo Expo, Vol. 2, Berlin, Germany, (2008), pp. 169–178.
[13] Mandache, C., Mcelhinney, T., Mrad, N. Aircraft Engine Blade Tip Monitoring Using Pulsed Eddy Current Technology, 4th International Symposium on NDT in Aerospace 2012 - Th.4.A.3.
[14] Karakoc, K., Suleman, A., Park, E-J. Analytical modeling of eddy current brakes with the application of time varying magnetic fields. Applied Mathematical Modeling 40, (2016), pp. 1168-1179.
[15] Rosell, A., Persson, G. Finite element modelling of closed cracks in eddy current testing. International Journal of Fatigue 41, (2012), pp. 30-38.
[16] Pohl, R., Erhard, A., Montag, H-J., Thomas, H-M., Wüstenberg, H. NDT techniques for railroad wheel and gauge corner inspection, NDT & E International, (37), (2004), 89-94.
[17] Weststrate, E., Steinback, M., Rensing, N-M., Tiernan, T. COMSOL Multiphysics Modeling for Design Optimization of Eddy Current Crack Detectors. Excerpt from the Proceedings of the COMSOL Conference 2010 Boston.